IEEE Access
Multidisciplinary | Rapid Review | Open Access Journal

Received November 30, 2021, accepted December 16, 2021, date of publication December 20, 2021,
date of current version January 20, 2022.

Digital Object Identifier 10.1109/ACCESS.2021.3136770

Quadrature Demodulation Method for Resolver Signal Processing Under Different Sampling Rate

POOREUM JANG, TAEYEON LEE, YUNKYUNG HWANG, AND KWANGHEE NAM, (Life Member, IEEE)
Department of Electrical Engineering, Pohang University of Science and Technology (POSTECH), Pohang 37673, South Korea
Corresponding author: Kwanghee Nam (kwnam@postech.ac.kr)

ABSTRACT Resolvers are widely used as position sensors to obtain angle information. The resolver requires the excitation signal and its amplitude is modulated by the rotor position. The envelope of the modulated signal can be detected precisely only when the samplings are synchronized with the excitation signal. A large error can occur if the synchronization fails. In this paper, the resolver signals are sampled in synchronization with the pulsewidth modulation (PWM) carrier, not the excitation signal. When the resolver excitation signal frequency and the PWM carrier frequency are different, the envelope cannot be detected, so additional signal processing is required to obtain the angle information. For signal processing, multiple auxiliary signals are synthesized based on the sampled signals and quadrature demodulation is performed. A detailed error analysis according to the PWM frequency and motor speed is also performed. The effectiveness is demonstrated through simulation and experimental evidence.

INDEX TERMS Phase-locked loop (PLL), resolver-to-digital conversion (RDC), demodulation, resolver, envelope detection.

I. INTRODUCTION

The accuracy of rotor position and speed measurements play the most important role in determining motor control performance [1], [3]. The methods of obtaining angle information are largely divided into two groups; using angle sensors and sensorless algorithms [4], [5]. Since the sensorless method does not use angle sensors, it is cost effective, but the angle sensors are still used in many fields for reasons of reliability, utility, and robustness. Among many angle sensors, resolvers are widely used due to their robustness and simple structure. When an excitation signal is applied to the resolver, amplitude-modulated sine and cosine signals are output. The phase-locked loop (PLL) [6]–[8] is used to obtain angle information via demodulation. The whole process of obtaining angle information from resolver signals is called resolver-to-digital conversion (RDC).

To detect envelope of the resolver signals, the signals are sampled at the peak of the excitation signal [9]–[11]. It is relatively simple to implement and has no delay associated with low pass filter. Because the sampling is synchronized with the excitation signal, it is called a synchronous sampling method or a peak sampling method. It is also called the under sampling method because the sampling frequency does not satisfy the Nyquist frequency. However, there is no flexibility to change the sampling frequency because it must sample at the peak of the excitation signal. A square wave excitation signal was used to give a more freedom in sampling timing [12], [13]. It allowed sampling at various points on the flat top of the square wave. However, it may suffer significant signal distortion caused by cable impedance mismatch and harmonic loss. Wang and Wu [14] utilized multiple sampling and a correction method to increase the RDC accuracy and to reduce quantization error.

There are also various studies to improve angle accuracy [15]–[17]. A look-up table (LUT) is usually used for trigonometric functions, but the LUT methods have some inconveniences such as data interpolation and memory space. Wang *et al.* [15] generated auxiliary sinusoidal signals by adding and subtracting the demodulated signals to increase the linearity. By utilizing the linearized signal, they could increase the position accuracy without a LUT. Similarly, Ye *et al.* [16] made multiple linear sections of the sinusoidal signal near the null points and used an array of phase-shifted signals to increase the linearity at the zero crossings. A third-order rational polynomial can be used in place of arc tangent

The associate editor coordinating the review of this manuscript and approving it for publication was Gautam Srivastava.

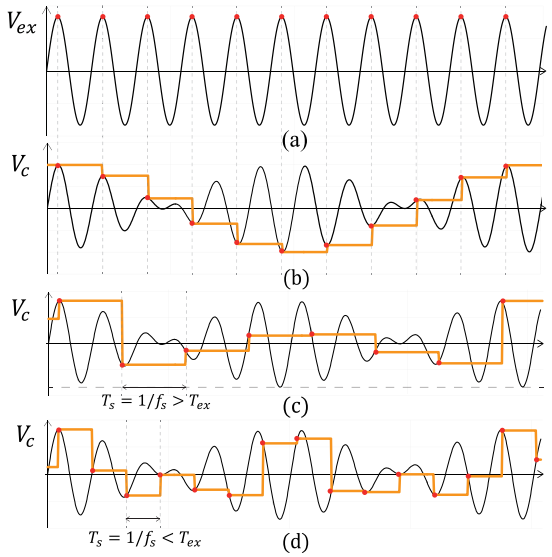

FIGURE 1. Resolver signal sampling of V_c with different sampling frequencies f_S: (a) excitation signal V_{ex}, (b) peak sampling $f_S = f_{ex}$, (c) $f_S > f_{ex}$, (d) $f_S < f_{ex}$.

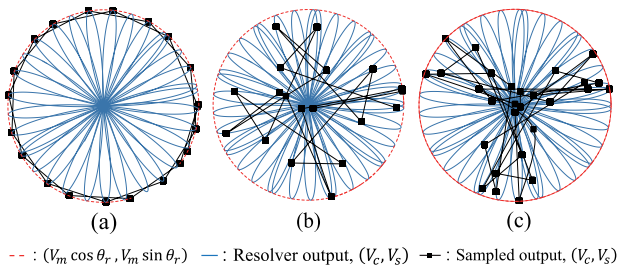

FIGURE 2. Lissajous curves of (V_c, V_S) with different f_S: (a) peak sampling $f_S = f_{ex}$, (b) $f_S = 0.8f_{ex}$, (c) $f_S = 1.3f_{ex}$.

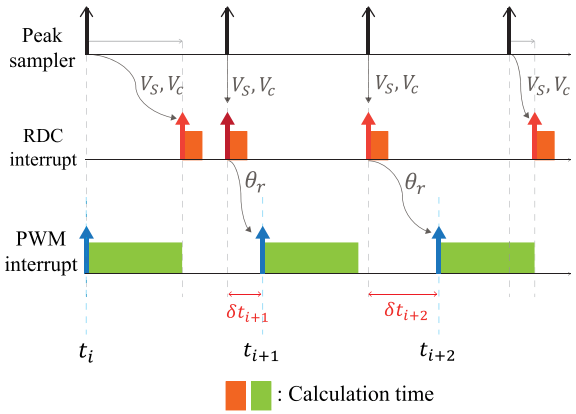

FIGURE 3. Timing diagram when RDC interrupts and PWM interrupts are performed separately.

function. Wang *et al.* [17] obtained pseudo-linear signals using the third-order rational polynomial and compensated the angle error through a polynomial fitting. However, since these methods are based on demodulated signals, there is no other mention of the demodulation method.

In motor control, angle information is required at the time of PWM interrupt. Usually, the resolver signals are sampled and processed in the PWM interrupt service routine (ISR). However, in this case, if the PWM frequency is different from that of the resolver excitation frequency, it will fail to sample at the peak of the excitation signal, causing problems in envelope detection. Therefore, an angle error occurs in the demodulation process due to synchronization mismatch. For this reason, in order to use the conventional RDC method based on synchronization, the PWM frequency must be matched to the resolver carrier frequency. Recently, variable frequency control [18] or changing the switching frequency for each specific torque/speed region is used to increase the efficiency, so there is a limitation to apply the existing RDC method.

In this study, a new RDC method for PWM frequency selection independent of the excitation signal frequency is proposed. The proposed method asynchronously samples the resolver signal according to the PWM frequency. Since the envelope is not detected properly, an extra signal processing is required. For this purpose, the resolver signals are sampled twice from one PWM period as double sampling [19]. Two sets of signals sampled at adjacent interrupt points are used to synthesize multiple auxiliary signals to obtain angular information.

This paper is organized as follows. In Section II, the peak sampling method is described and several problems are discussed when the sampling frequency and the excitation signal frequency are different. In Section III, the proposed demodulation method is illustrated with definitions of new variables. Section IV shows simulation and experiment results.

II. RESOLVER SIGNAL SAMPLING BASED ON PWM

A resolver is a kind of transducer that requires an excitation signal V_{ex} as input. The two output signals are modulated with a sine wave V_s and a cosine wave V_c depending on the rotor angle [20]:

$$V_{ex} = U_m \sin \omega_{ex} t, \tag{1}$$

$$V_s = V_m \sin \omega_{ex} t \ \sin\theta_r - \frac{\omega_r}{\omega_{ex}} V_m \cos \omega_{ex} t \ \cos\theta_r, \tag{2}$$

$$V_c = V_m \sin \omega_{ex} t \ \cos\theta_r + \frac{\omega_r}{\omega_{ex}} V_m \cos \omega_{ex} t \ \sin\theta_r, \tag{3}$$

where U_m and V_m are the amplitudes of excitation and output signals, $\omega_{ex} = 2\pi f_{ex}$ and ω_r are the angular speeds of the excitation signal and motor, and $\theta_r = \omega_r t$ is the rotor position. Generally, ω_{ex} is much larger than ω_r, so the last terms in (2) and (3) are ignored.

The peak sampling method is simple and robust because it is an under-sampling method [9]–[11]. Figs. 1 (a) and (b) show the excitation signal V_{ex} and a modulated output signal V_c. With peak sampling, V_c is sampled at the peak of the excitation signal, yielding the envelope of cosine signal. Fig. 1 (c) shows an example of irregular sampling when the excitation frequency is higher than the sampling frequency,

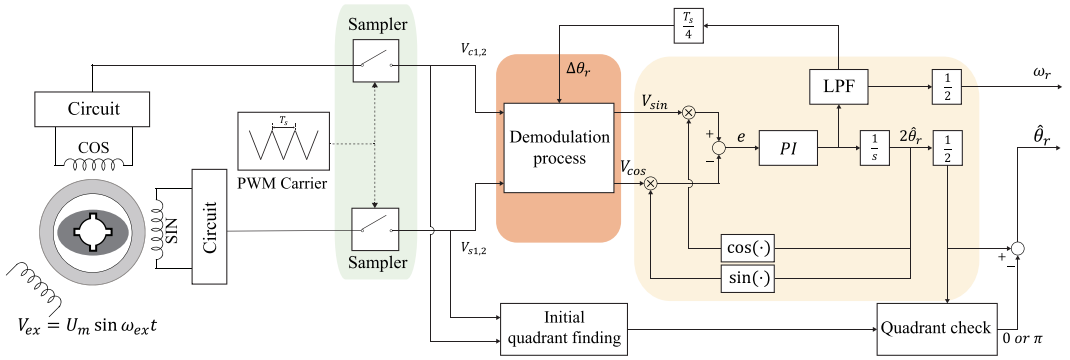

FIGURE 4. The overall block diagram of the proposed demodulation method.

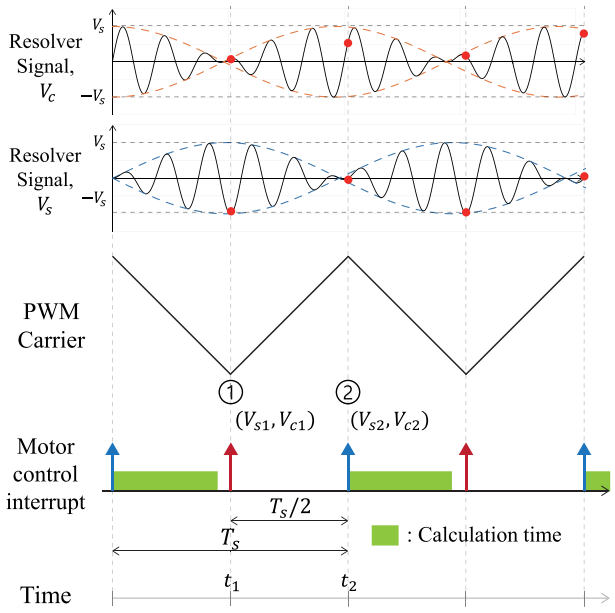

FIGURE 5. PWM carrier and sampled resolver signals at t_1 and t_2.

$f_{ex}/f_s = 1.4$. Fig. 1 (d) shows the other example when the sampling frequency is higher than the excitation frequency, $f_{ex}/f_s = 0.8$. In both cases, the sampled signals are far from the sine and cosine shapes. Fig. 2 (a) shows the Lissajous curve when V_s and V_c are sampled at the peak. Note that the sampled points lie regularly on the red circle with the peak sampling. Figs. 2 (b) and (c) show the corresponding Lissajous curves when the sampling is not taken at the peak, in which the sampled points are randomly displaced from the circle. As shown in the above, if the sampling frequency is not an integer ratio of the carrier frequency, i.e. $\frac{f_s}{f_{ex}} \neq \frac{1}{n}$, where n is an integer, a large angle error may occur.

Fig. 3 shows the timing diagram when RDC and PWM interrupt are used separately. The first row shows the timing of the peak sampling. The second and third rows show the RDC and PWM interrupts and calculation times, respectively. If the PWM interrupt has the highest priority, the RDC ISR to obtain the angle information is always delayed until the PWM ISR completes. At t_{i+1}, delayed sampled data $\theta_r(t_{i+1} - \delta t_{i+1})$ is used for $(i+1)$th PWM interrupt. That is, the angle used at the $(i+1)$th PWM interrupt is the last calculated angle from the RDC interrupt. Since the calculation time used for PWM and RDC interrupt is not always constant, δt_i is not constant. Such varying delays cause the following moving average error:

$$E_k = \frac{1}{K+1} \sum_{i=k}^{k+K} [\theta_r(t_i) - \theta_r(t_i - \delta t_i)]^2 , \tag{4}$$

where K is the size of moving window. If the calculation time of the PWM interrupt is longer, the error increases because the RDC interrupt is not properly executed.

A. PROPOSED RDC PROCESSING

The overall algorithm proposed in this paper is well shown in Fig. 4. The resolver outputs V_s and V_c are sampled in synchronization with the PWM carrier, and V_{sin} and V_{cos} are output by correcting the error caused by non-peak sampling in the demodulator. They are also applied as inputs to the quadrature PLL to determine the angle. Since V_{sin} and V_{cos} have double angle frequencies, it is necessary to check the initial quadrant. In this paper, it is assumed that the resolver output signals are sampled twice per PWM period as double sampling [19].

Fig. 5 shows two resolver output signals and the PWM carrier. The PWM period is denoted by T_s, and (V_{s1}, V_{c1}) and (V_{s2}, V_{c2}) are sampled at t_1 and t_2 respectively. Since they are sampled at regular intervals, the time interval between t_1 and t_2 is $T_s/2$, i.e., $t_2 - t_1 = T_s/2$. The two sampled data sets are

$$V_{s1} = V_m \sin\theta_{ex1} \sin\theta_{r1}, \tag{5}$$
$$V_{c1} = V_m \sin\theta_{ex1} \cos\theta_{r1}, \tag{6}$$
$$V_{s2} = V_m \sin\theta_{ex2} \sin\theta_{r2}, \tag{7}$$
$$V_{c2} = V_m \sin\theta_{ex2} \cos\theta_{r2}, \tag{8}$$

where $\theta_{ex1} = \theta_{ex}(t_1)$, $\theta_{r1} = \theta_r(t_1)$, $\theta_{ex2} = \theta_{ex}(t_2) = \theta_{ex}(t_1 + T_s/2)$, and $\theta_{r2} = \theta_r(t_1 + T_s/2)$. Assuming ω_r is constant within short PWM periods, $\theta_{r2} = \theta_r(t_1) + \omega_r T_s/2$. Let the incremental angle over a half PWM interval $T_s/2$ in

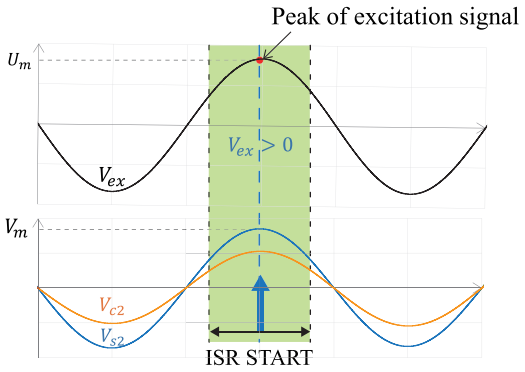

FIGURE 6. Timing of first PWM interrupt for initial quadrant determination.

the excitation and resolver signals be defined by $\Delta\theta_{ex} = \theta_{ex2} - \theta_{ex1} = (\omega_{ex}T_s)/2$ and $\Delta\theta_r = \theta_{r2} - \theta_{r1} = (\omega_r T_s)/2$.

B. QUADRATURE DEMODULATION

Equations (7) and (8) can be expressed equivalently as [21]

$$V_{s2} = -\frac{V_m}{2}\left[\cos(\theta_{ex2} + \theta_{r2}) - \cos(\theta_{ex2} - \theta_{r2})\right], \quad (9)$$

$$V_{c2} = \frac{V_m}{2}\left[\sin(\theta_{ex2} + \theta_{r2}) + \sin(\theta_{ex2} - \theta_{r2})\right]. \quad (10)$$

Let $x_{2p} = \cos(\theta_{ex2} + \theta_{r2})$, $x_{2n} = \cos(\theta_{ex2} - \theta_{r2})$, $y_{2p} = \sin(\theta_{ex2} + \theta_{r2})$ and $y_{2n} = \sin(\theta_{ex2} - \theta_{r2})$. Suppose that these four components are known individually then utilizing trigonometric formula, it follows that

$$\cos 2\theta_{r2} = x_{2p}x_{2n} + y_{2p}y_{2n}, \quad (11)$$

$$\sin 2\theta_{r2} = x_{2n}y_{2p} - x_{2p}y_{2n}. \quad (12)$$

The process shown in (11) and (12) is a kind of demodulation method because the excitation signal is deleted and only the sine and cosine functions of $2\theta_{r2}$ remain. The angle information is obtained by the quadrature PLL or using the inverse tangent function such that

$$\theta_{r2} = \frac{1}{2}\tan^{-1}\left(\frac{x_{2n}y_{2p} - x_{2p}y_{2n}}{x_{2p}x_{2n} + y_{2p}y_{2n}}\right). \quad (13)$$

As shown in (13), four components composing V_{s2} and V_{c2} should be found. To find the four components, two separate expressions are needed. These two additional expressions are obtained by interpolating (V_{s1}, V_{c1}) at t_1 to t_2.

As a first step, define new variables using (V_{s1}, V_{c1}) and (V_{s2}, V_{c2}):

$$V_{a2} \equiv -V_{s1} + \cos\Delta\theta_{ex}\left[V_{s2}\cos\Delta\theta_r - V_{c2}\sin\Delta\theta_r\right], \quad (14)$$

$$V_{b2} \equiv -V_{c1} + \cos\Delta\theta_{ex}\left[V_{s2}\sin\Delta\theta_r + V_{c2}\cos\Delta\theta_r\right]. \quad (15)$$

Using the identities $\sin\theta_{ex1} = \sin(\theta_{ex2} - \Delta\theta_{ex})$, $\sin\theta_{r1} = \sin(\theta_{r2} - \Delta\theta_r)$ and $\cos\theta_{r1} = \cos(\theta_{r2} - \Delta\theta_r)$, it follows that

$$V_{a2} = V_{s\Delta}\cos\theta_{ex2}\sin\theta_{r1}, \quad (16)$$

$$V_{b2} = V_{s\Delta}\cos\theta_{ex2}\cos\theta_{r1}, \quad (17)$$

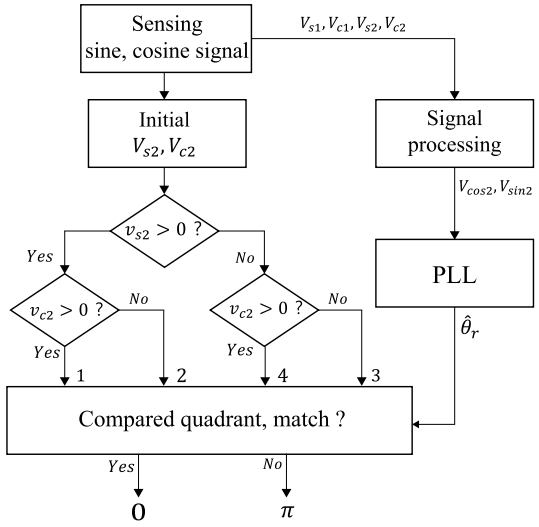

FIGURE 7. Flow chart for initial quadrant determination.

where $V_{s\Delta} \equiv V_m \sin\Delta\theta_{ex}$. Unlike (7) and (8) which have a sine excitation signal, $\sin\theta_{ex}$, (16) and (17) are amplitude modulated signals which have a cosine excitation signal, $\cos\theta_{ex}$. Since the demodulation utilizes both cosine and sine excitation signals, it is called here 'quadrature demodulation.'

Using V_{s2}, V_{c2}, V_{a2} and V_{b2}, define new variables additionally:

$$X_{2p} \equiv V_{b2} - \sin\Delta\theta_{ex}\cos\Delta\theta_r V_{s2} - \tan\Delta\theta_r V_{a2}, \quad (18)$$

$$X_{2n} \equiv V_{b2} + \sin\Delta\theta_{ex}\cos\Delta\theta_r V_{s2} - \tan\Delta\theta_r V_{a2}, \quad (19)$$

$$Y_{2p} \equiv V_{a2} + \sin\Delta\theta_{ex}\cos\Delta\theta_r V_{c2} + \tan\Delta\theta_r V_{b2}, \quad (20)$$

$$Y_{2n} \equiv -V_{a2} + \sin\Delta\theta_{ex}\cos\Delta\theta_r V_{c2} - \tan\Delta\theta_r V_{b2}. \quad (21)$$

Substituting (7), (8), (14), and (15) into (18)-(21), it follows that

$$X_{2p} = \mathcal{C}\left[\cos(\theta_{ex2} + \theta_{r2}) + \tan^2\Delta\theta_r\cos\theta_{ex2}\cos\theta_{r2}\right], \quad (22)$$

$$X_{2n} = \mathcal{C}\left[\cos(\theta_{ex2} - \theta_{r2}) + \tan^2\Delta\theta_r\cos\theta_{ex2}\cos\theta_{r2}\right], \quad (23)$$

$$Y_{2p} = \mathcal{C}\left[\sin(\theta_{ex2} + \theta_{r2}) + \tan^2\Delta\theta_r\cos\theta_{ex2}\sin\theta_{r2}\right], \quad (24)$$

$$Y_{2n} = \mathcal{C}\left[\sin(\theta_{ex2} - \theta_{r2}) - \tan^2\Delta\theta_r\cos\theta_{ex2}\sin\theta_{r2}\right], \quad (25)$$

where $\mathcal{C} = V_m\sin\Delta\theta_{ex}\cos\Delta\theta_r$. Note that $\Delta\theta_r = \omega_r T_s/2$ is usually a small value, since it is a angle variation over a half PWM interval. Furthermore, $\tan^2\Delta\theta_r \approx \Delta\theta_r^2 \approx 0$ for small $\Delta\theta_r$. Therefore, the second terms in (22)-(25) can be neglected. Likewise (11)-(12), sine and cosine signals are obtained as

$$V_{cos2} \equiv X_{2p}X_{2n} + Y_{2p}Y_{2n} \approx \mathcal{C}^2\cos 2\theta_{r2}, \quad (26)$$

$$V_{sin2} \equiv X_{2n}Y_{2p} - X_{2p}Y_{2n} \approx \mathcal{C}^2\sin 2\theta_{r2}. \quad (27)$$

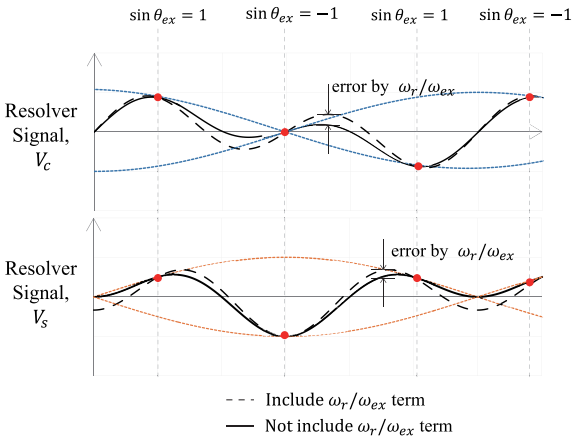

FIGURE 8. Error caused by ω_r/ω_{ex} in non peak sampling.

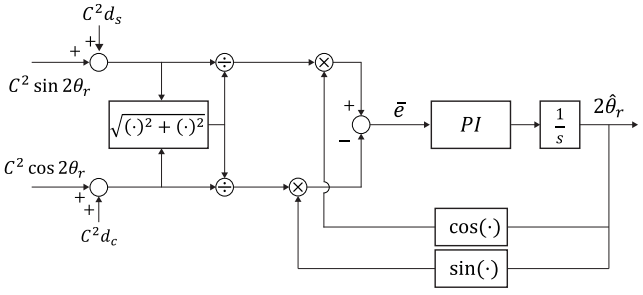

FIGURE 9. The PLL input perturbations, d_s and d_c due to ω_r/ω_{ex} and $\tan^2 \Delta\theta_r$.

The excitation component is completely removed from (26)-(27), leaving only the rotor angle information.

In estimating $2\theta_r$, the quadrature PLL shown in Fig. 4 [8] is used by applying V_{cos2} and V_{sin2} to the inputs. The input of PI regulator is expressed as follows:

$$e = \frac{1}{\sqrt{V_{sin2}^2 + V_{cos2}^2}} \left[V_{sin2} \cos 2\hat{\theta}_r - V_{cos2} \sin 2\hat{\theta}_r \right] \approx \sin(2\theta_r - 2\hat{\theta}_r) \approx 2\theta_r - 2\hat{\theta}_r. \quad (28)$$

$2\hat{\theta}_r$ is detected which makes $e = 0$ by the PI regulator.

C. POLARITY DETECTION

In order to obtain the desired angle θ_r from $2\theta_r$, it is important to determine the initial quadrant [22], [23]. The angle should be chosen with the aid of $\sin\theta_r$ and $\cos\theta_r$, and these signals are contained in V_{s2} and V_{c2}. In (7) and (8), if the excitation component $\sin\theta_{ex2}$ is positive, the desired signs of $\sin\theta_r$ and $\cos\theta_r$ are the same as V_{s2} and V_{c2}, respectively. Based on this concept, it is proposed to detect the initial quadrant of θ_r by starting the first PWM interrupt at the $V_{ex} > 0$ as shown in Fig. 6.

Fig. 7 illustrates the initial quadrant detection process. One of four quadrants is found using the sensed signs of V_{s2} and V_{c2} at first interrupt. If this value does not match the quadrant of the output angle from the PLL, π is added, and if it does match, 0 is added. The first interrupt only needs to start at any point where the excitation signal is positive. This means more degrees of freedom compared to the peak sampling method.

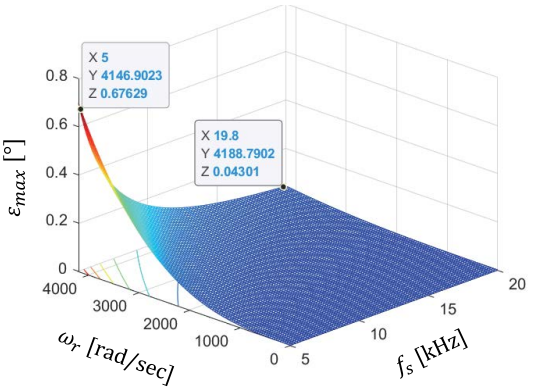

FIGURE 10. Angular error, ε according to sampling frequency, f_s and motor angular velocity ω_r.

TABLE 1. Parameters of IPMSM.

Name	Value	Unit
Rated power	7.5	kW
Switching frequency	7-15	kHz
Rated torque	5	Nm
Rated speed	3800	rpm
DC-link voltage	150	V
ψ_m	0.06684	Wb
D-axis inductance, L_d	1.18	mH
Q-axis inductance, L_q	2.23	mH
Number of pole, P	4	
Excitation frequency, f_{ex}	10	kHz

III. ERROR ANALYSIS

In the previous section, ω_r/ω_{ex} and $\tan^2\Delta\theta_r$ have been ignored for simplicity's sake. However, this section analyzes their effect on angle errors. First, it is worth observing how the motor speed affects the resolver signals when not sampling at the peak of the excitation signal. Fig. 8 shows the modulated signals (2) and (3) with and without terms including ω_r/ω_{ex}. As indicated by red marks the sampled data are not affected by ω_r/ω_{ex} when the sampling is made at the peaks of $\sin\theta_{ex}$. It is because $\cos\theta_{ex} = 0$ whenever $|\sin\theta_{ex}| = 1$. However, ω_r/ω_{ex} will have an effect if the sampling is not made at the peak. It will cause an angle error and its effect grows in proportion to ω_r.

In addition, although the demodulation signals (22)-(25) contain $\tan^2\Delta\theta_r$, it was neglected by assuming $\tan^2\Delta\theta_r \approx 0$ over a half PWM period $T_s/2$. But as the motor speed increases, its magnitude gradually increases.

Including all, it follows from (18)-(21) that

$$\bar{X}_{2p,n} = \mathcal{C}\left[\left(1 \pm \frac{\omega_r}{\omega_{ex}}\right) \cos(\theta_{ex2} + \theta_{r2}) + \tan^2\Delta\theta_r \times \left(\cos\theta_{ex2}\cos\theta_{r2} - \frac{\omega_r}{\omega_{ex}} \sin\theta_{ex2}\sin\theta_{r2} \right) \right], \quad (29)$$

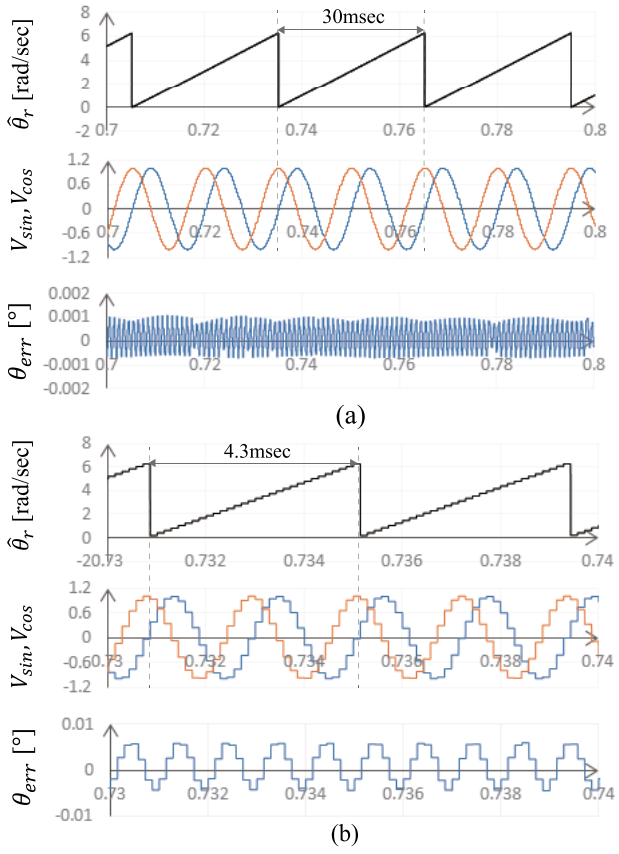

FIGURE 11. Simulation results at f_s = 7kHz: (a) 1000rpm, (b) 7000rpm.

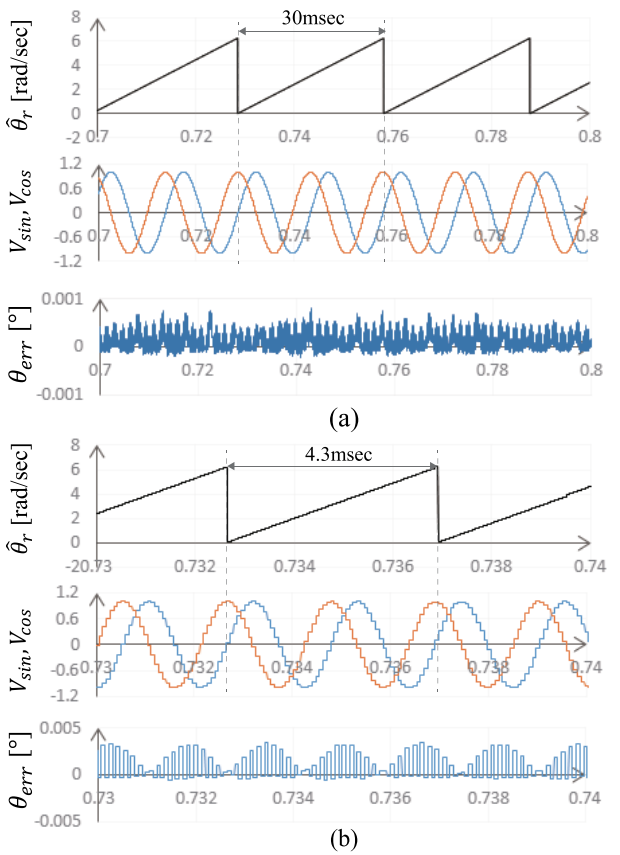

FIGURE 12. Simulation results at f_s = 13kHz: (a) 1000rpm, (b) 7000rpm.

$$\bar{Y}_{2p,n} = \mathcal{C}\Bigg[\left(1 \pm \frac{\omega_r}{\omega_{ex}}\right)\sin\left(\theta_{ex2} - \theta_{r2}\right) \pm \tan^2\Delta\theta_r \times \left(\cos\theta_{ex2}\sin\theta_{r2} + \frac{\omega_r}{\omega_{ex}}\sin\theta_{ex2}\cos\theta_{r2}\right)\Bigg]. \tag{30}$$

Similarly to (26) and (27), we have

$$\bar{V}_{cos2} = \mathcal{C}^2\left[\cos 2\theta_{r2} + d_c\right], \tag{31}$$

$$\bar{V}_{sin2} = \mathcal{C}^2\left[\sin 2\theta_{r2} + d_s\right]. \tag{32}$$

The perturbations in (31) and (32) are expressed as

$$\begin{aligned} d_c = {} & k_0\left(1 + \frac{\omega_r^2}{\omega_{ex}^2}\right)\cos 2\theta_{ex2}\cos 2\theta_{r2} \\ & -2\frac{\omega_r}{\omega_{ex}}k_0\sin 2\theta_{ex2}\sin 2\theta_{r2} \\ & +\left(k_0 - \frac{\omega_r^2}{\omega_{ex}^2}\left(1 + k_0\right)\right)\cos 2\theta_{r2}, \end{aligned} \tag{33}$$

$$\begin{aligned} d_s = {} & k_0\left(1 + \frac{\omega_r^2}{\omega_{ex}^2}\right)\cos 2\theta_{ex2}\sin 2\theta_{r2} \\ & +2\frac{\omega_r}{\omega_{ex}}k_0\sin 2\theta_{ex2}\cos 2\theta_{r2} \\ & +\left(k_0 - \frac{\omega_r^2}{\omega_{ex}^2}\left(1 + k_0\right)\right)\sin 2\theta_{r2}, \end{aligned} \tag{34}$$

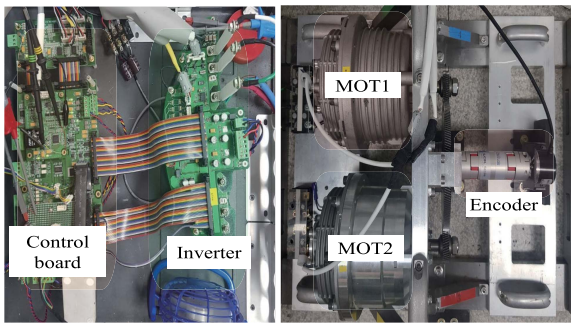

FIGURE 13. PMSM and inverter used in experiments.

where $k_0 = \tan^2\Delta\theta_r(1 + 0.5\tan^2\Delta\theta_r)$. These are applied to the PLL as shown in Fig. 9. Then the input of the PI regulator, $\bar{e}$ is obtained from (31)-(34) such that

$$\begin{aligned} \bar{e} &= \frac{\mathcal{C}^2 k_2}{\sqrt{\bar{V}_{sin2}^2 + \bar{V}_{cos2}^2}}\left[\sin\left(2\theta_{r2} - 2\hat{\theta}_r\right) + \frac{k_1}{k_2}\cos\left(2\theta_{r2} - 2\hat{\theta}_r\right)\right] \\ &\approx \frac{\mathcal{C}^2 k_2}{\sqrt{\bar{V}_{sin2}^2 + \bar{V}_{cos2}^2}}\left[2(\theta_{r2} - \hat{\theta}_r) + \varepsilon\right], \end{aligned} \tag{35}$$

where $\varepsilon = k_1/k_2$, $k_1 = 2\omega_r/\omega_{ex}k_0\sin 2\theta_{ex2}$ and $k_2 = \left(1 - \omega_r^2/\omega_{ex}^2\right)\left(k_0 + 1\right) + \left(1 + \omega_r^2/\omega_{ex}^2\right)k_0\cos 2\theta_{ex2}$. Note

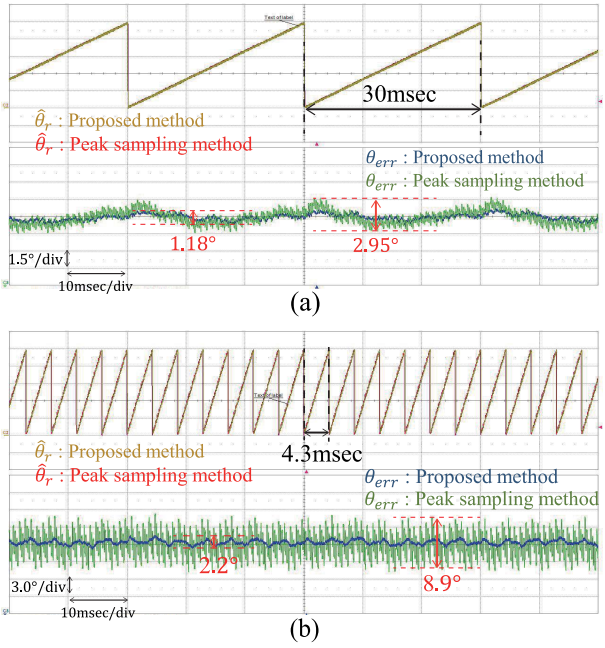

FIGURE 14. Comparison with the peak sampling method when the switching frequency is 7 kHz: (a) 1000 rpm, (b) 7000 rpm.

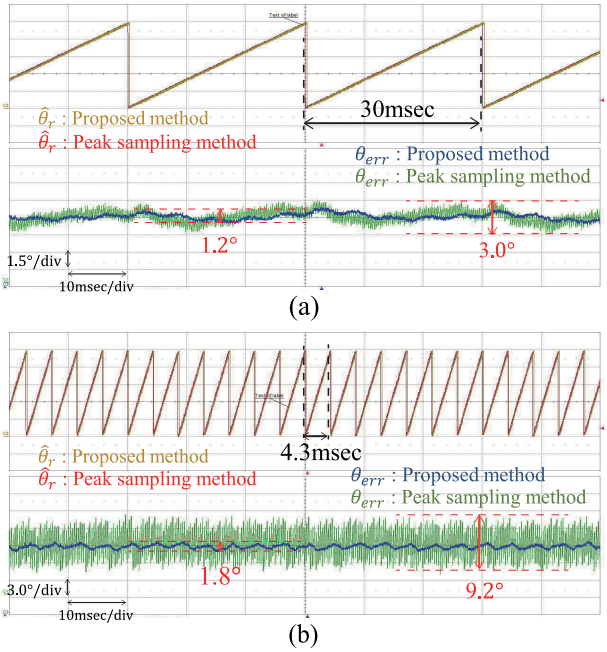

FIGURE 15. Comparison with the peak sampling method by speed when the switching frequency is 13kHz: (a) 1000 rpm, (b) 7000 rpm.

that ε is the perturbing error that is caused by ω_r/ω_{ex} and $\tan^2 \Delta\theta_r$. So its upper bound is obtained by differentiating it with respect to $2\theta_{ex}$ such as

$$\varepsilon_{max} = \frac{2k_0\omega_r\omega_{ex}\sqrt{(2k_0+1)(\omega_{ex}^2-\omega_r^2)^2 - 4k_0^2\omega_{ex}^2\omega_r^2}}{(\omega_{ex}^2-\omega_r^2)^2(1+k_0)^2 - (\omega_{ex}^2+\omega_r^2)^2k_0^2}. \tag{36}$$

Fig. 10 shows the plot of ε_{max} over the plain of ω_r and f_s, when $f_{ex} = 10$kHz. As expected from (36), the error ε_{max} increases along with the motor speed ω_r, and decreases as the switching frequency f_s increases. The maximum error occurs at a switching frequency of 5 kHz and a speed corresponding to 20000 rpm based on a 4-pole motor. According to this analysis, the angle error is less than 0.7° in the entire range.

The maximum angle error ε_{max} according to f_s and motor speed ω_r is examined. But actually in (31) and (32), $\mathcal{C}^2$ equals 0 when $T_s/T_{ex} = m$ for an integer m, so V_{cos2} and V_{sin2} will also become 0. Therefore, the proposed demodulation method has a disadvantage in that it cannot use a sampling frequency that is a multiple of the excitation signal frequency, but has the advantage of more flexibility in frequency selection compared to the peak sampling method.

IV. SIMULATION AND EXPERIMENTAL RESULTS

The motor parameters used in the experiments and simulations are listed in Table.1. Simulation was conducted through MATLAB/SIMULINK. Fig. 13 shows the PMSM and inverter used in this experiment. The TI TMS320F28377D was used for DSP. The circuit [24] for the resolver excitation signal was used and the bandwidth of the PLL was set at 700 Hz. For comparison, an encoder was used which outputs 6000 pulses per revolution. The effectiveness of the proposed method was verified by the angle error θ_{err} between the actual angle and the angle obtained by the proposed method. In the actual experiment, θ_{err} was calculated as the difference between the angle obtained by the encoder and the proposed angle.

Figs. 11 and 12 show the speed control simulation results when f_s is 7 kHz and 13 kHz using the proposed method. Figs. 11 (a) and (b) show the PLL output $\hat{\theta}_r$ and the PLL inputs V_{cos}, V_{sin}, and the angle error θ_{err} when $f_s = 7$ kHz and the motor speed is 1000 and 7000 rpm, respectively. Similar results are shown in Figs. 12 (a) and (b) show the similar simulation result when $f_s = 13$ kHz. Note that θ_{err} is limited to $\pm 0.001°$ at 1000 rpm and $\pm 0.05°$ at 7000 rpm, which are a small value despite sampling asynchronous to the resolver excitation signal. As was predicted in (36), the error becomes small as the motor speed decreases and the PWM frequency increases.

Figs. 14 and 15 show the experimental results of the proposed method when $f_s = 7$ kHz and 13 kHz, respectively. A separate interrupt for the peak sampling method was used and compared with the proposed method. The θ_{err} (blue) of the proposed method at 1000 rpm is not significantly different from θ_{err} (green) of the peak sampling method. However, the difference is much larger at 7000 rpm. This is because, as shown in Fig 3, the changing angle during the time difference δt between RDC for peak sampling and PWM interrupt increases with speed. The same experimental results is shown in Fig.15 when $f_s = 13$ kHz. It can be seen that the proposed method shows a smaller error when f_s is higher, which is

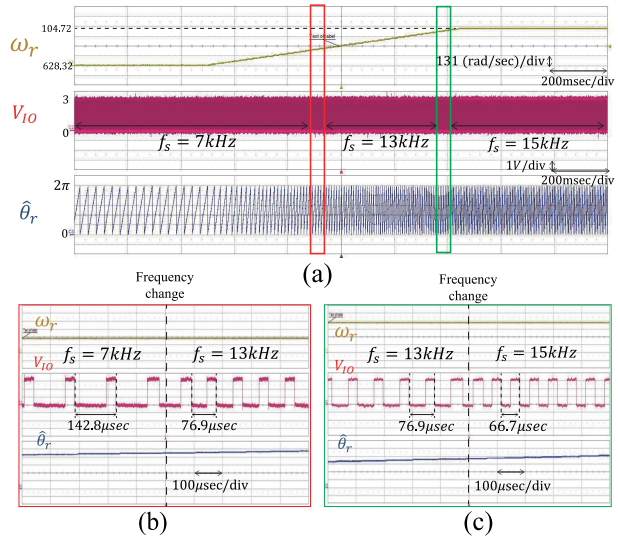

FIGURE 16. Speed control with the quadrature demodulation under different PWM (sampling) frequencies when the motor speed increases from 1000 rpm to 5000 rpm: (a) motor speed ω_r, IO voltage V_{IO} indicating the start of ISR, and angle estimate $\hat{\theta}_r$, (b) zoom-in plot when f_s changes from 7 kHz to 13 kHz, (c) zoom-in plot when f_s changes from 13 kHz to 15 kHz.

in good agreement with the error analysis result mentioned above. Even the same calculation time, it occupies a relatively large portion as the PWM period becomes shorter. So the case of 13 kHz has larger error than the case of 7 kHz when the peak sampling method was applied. In Figs.14 and 15, there are angular errors corresponding to the fundamental and double frequencies. This may occur for various reasons such as the scaling, quadrature, and offset errors of the resolver signals [25], or offset and scaling error of the sensed current [26], but the methods of eliminating errors due to these factors are beyond the scope of this paper.

Fig. 16 (a) shows the motor speed ω_r, input/output (IO) signal V_{IO} indicating the start of ISR, and the PLL output $\hat{\theta}_r$ when the f_s changes from 7 kHz to 15 kHz. Note that the motor speed increases from 1000 rpm to 5000 rpm. At 3000 rpm, the PWM frequency changes from 7 kHz to 13 kHz. Also, at 5000 rpm, the PWM frequency changes from 13 kHz to 15 kHz. Figs. 16 (b) and (c) are expanded waveforms, in which the differences in PWM periods are clearly seen. This shows that the motor speed control performs well when the PWM frequency is changed. In the peak sampling method, it is impossible to change the frequency because it must be synchronized with the peak of the excitation signal, but it can be seen that the PWM frequency can be changed in the proposed RDC method.

V. CONCLUSION

A demodulation method based on resolver signals sampled in synchronization with a PWM interrupt is proposed. This method is called 'quadrature demodulation' because it additionally generates a pair of signals modulated with a cosine excitation signal. Quadrature demodulation is performed using the sine and cosine excitation signals and the results are applied to the input of quadrature PLL. This method is very suitable for motor current control because it samples the resolver signals in synchronization with the PWM interrupt. Although a frequency corresponding to a multiple of the excitation signal cannot be used, the frequency selection is more free compared to the existing method. In addition, the maximum value of the angle error that can occur when the motor speed is high was calculated. The effectiveness is verified through simulation and experimental results.

REFERENCES

[1] J. Lara, J. Xu, and A. Chandra, "Effects of rotor position error in the performance of field-oriented-controlled PMSM drives for electric vehicle traction applications," *IEEE Trans. Ind. Electron.*, vol. 63, no. 8, pp. 4738–4751, Aug. 2016.

[2] S. Chen, Y. Zhao, H. Qiu, and X. Ren, "High-precision rotor position correction strategy for high-speed permanent magnet synchronous motor based on resolver," *IEEE Trans. Power Electron.*, vol. 35, no. 9, pp. 9716–9726, Sep. 2020.

[3] D. Chen, J. Li, J. Chen, and R. Qu, "On-line compensation of resolver periodic error for PMSM drives," *IEEE Trans. Ind. Appl.*, vol. 55, no. 6, pp. 5990–6000, Nov./Dec. 2019.

[4] J. Choi, K. Nam, A. A. Bobtsov, and R. Ortega, "Sensorless control of IPMSM based on regression model," *IEEE Trans. Power Electron.*, vol. 34, no. 9, pp. 9191–9201, Sep. 2019.

[5] S.-C. Yang and Y.-L. Hsu, "Full speed region sensorless drive of permanent-magnet machine combining saliency-based and back-EMF-based drive," *IEEE Trans. Ind. Electron.*, vol. 64, no. 2, pp. 1092–1101, Feb. 2017.

[6] T. N.-C. Tran, H. X. Nguyen, J. W. Park, and J. W. Jeon, "Improving the accuracy of an absolute magnetic encoder by using harmonic rejection and a dual-phase-locked loop," *IEEE Trans. Ind. Electron.*, vol. 66, no. 7, pp. 5476–5486, Jul. 2019.

[7] M. Guo, Z. Wu, and H. Qin, "Harmonics reduction for resolver-to-digital conversion via second-order generalized integrator with frequency-locked loop," *IEEE Sensors J.*, vol. 21, no. 6, pp. 8209–8217, Mar. 2021.

[8] F. Wang, T. Shi, Y. Yan, Z. Wang, and C. Xia, "Resolver-to-digital conversion based on acceleration-compensated angle tracking observer," *IEEE Trans. Instrum. Meas.*, vol. 68, no. 10, pp. 3494–3502, Oct. 2019.

[9] D. A. Khaburi, "Software-based resolver-to-digital converter for DSP-based drives using an improved angle-tracking observer," *IEEE Trans. Instrum. Meas.*, vol. 61, no. 4, pp. 922–929, Apr. 2012.

[10] M. Caruso, A. O. Di Tommaso, F. Genduso, R. Miceli, and G. R. Galluzzo, "A DSP-based resolver-to-digital converter for high-performance electrical drive applications," *IEEE Trans. Ind. Electron.*, vol. 63, no. 7, pp. 4042–4051, Jul. 2016.

[11] N. A. Qamar, C. J. Hatziadoniu, and H. Wang, "Speed error mitigation for a DSP-based resolver-to-digital converter using autotuning filters," *IEEE Trans. Ind. Electron.*, vol. 62, no. 2, pp. 1134–1139, Feb. 2015.

[12] T. Shi, Y. Hao, G. Jiang, Z. Wang, and C. Xia, "A method of resolver-to-digital conversion based on square wave excitation," *IEEE Trans. Ind. Electron.*, vol. 65, no. 9, pp. 7211–7219, Sep. 2018.

[13] V. Sabatini, M. Di Benedetto, and A. Lidozzi, "Synchronous adaptive resolver-to-digital converter for FPGA-based high-performance control loops," *IEEE Trans. Instrum. Meas.*, vol. 68, no. 10, pp. 3972–3982, Oct. 2019.

[14] K. Wang and Z. Wu, "Oversampling synchronous envelope detection for resolver-to-digital conversion," *IEEE Trans. Ind. Electron.*, vol. 67, no. 6, pp. 4867–4876, Jun. 2020.

[15] Y. Wang, Z. Zhu, and Z. Zuo, "A novel design method for resolver-to-digital conversion," *IEEE Trans. Ind. Electron.*, vol. 62, no. 6, pp. 3724–3731, Jun. 2015.

[16] G. Ye, G. Zhao, H. Liu, and B. Lu, "Precise phase demodulation algorithm for sinusoidal encoders and resolvers," *IEEE Trans. Ind. Electron.*, vol. 67, no. 10, pp. 8778–8787, Oct. 2020.

[17] S. Wang, J. Kang, M. Degano, and G. Buticchi, "A resolver-to-digital conversion method based on third-order rational fraction polynomial approximation for PMSM control," *IEEE Trans. Ind. Electron.*, vol. 66, no. 8, pp. 6383–6392, Aug. 2019.
[18] F. Yang, A. R. Taylor, H. Bai, B. Cheng, and A. A. Khan, "Using d–q transformation to vary the switching frequency for interior permanent magnet synchronous motor drive systems," *IEEE Trans. Transport. Electrific.*, vol. 1, no. 3, pp. 277–286, Oct. 2015.
[19] J. Kim and J. S. Lai, "Quad sampling incremental inductance measurement through current loop for switched reluctance motor," *IEEE Trans. Instrum. Meas.*, vol. 69, no. 7, pp. 4251–4257, Jul. 2020.
[20] D. C. Hanselman, "Resolver signal requirements for high accuracy resolver-to-digital conversion," *IEEE Trans. Ind. Electron.*, vol. 37, no. 6, pp. 556–561, Dec. 1990.
[21] J. Bergas-Jané, C. Ferrater-Simón, G. Gross, R. Ramírez-Pisco, S. Galceran-Arellano, and J. Rull-Duran, "High-accuracy all-digital resolver-to-digital conversion," *IEEE Trans. Ind. Electron.*, vol. 59, no. 1, pp. 326–333, Jan. 2012.
[22] Z. Wang, Z. Cao, and Z. He, "Improved fast method of initial rotor position estimation for interior permanent magnet synchronous motor by symmetric pulse voltage injection," *IEEE Access*, vol. 8, pp. 59998–60007, 2020.
[23] K. Lin, P. Wang, P. Cai, X. Wu, and M. Lin, "Fast initial rotor position estimation for IPMSM with unipolar sequence-pulse injection," *IEEE Trans. Energy Convers.*, vol. 36, no. 4, pp. 3545–3554, Dec. 2021, doi: 10.1109/TEC.2021.3087646.
[24] *Using the Resolver Interface eTPU Function*, document AN3943 Rev. 0, Andrzej Lara System Application Engineer and Roznov Czech System Center, Freescale Semiconductor, Oct. 2009.
[25] C. W. Secrest, J. S. Pointer, M. R. Buehner, and R. D. Lorenz, "Improving position sensor accuracy through spatial harmonic decoupling, and sensor scaling, offset, and orthogonality correction using self-commissioning MRAS methods," *IEEE Trans. Ind. Appl.*, vol. 51, no. 6, pp. 4492–4504, Nov./Dec. 2015.
[26] M. Kim, S.-K. Sul, and J. Lee, "Compensation of current measurement error for current-controlled PMSM drives," *IEEE Trans. Ind. Appl.*, vol. 50, no. 5, pp. 3365–3373, Sep. 2014.

POOREUM JANG was born in Yeosu, South Korea, in 1993. He received the B.S. degree in electrical engineering from Pusan National University, Pusan, South Korea, in 2017, and the M.S. degree in electrical engineering from the Pohang University of Science and Technology (POSTECH), Pohang, South Korea, in 2019, where he is currently pursuing the Ph.D. degree.

His current research interests include AC motor control, electric vehicle, and power converter.

TAEYEON LEE was born in South Korea, in 1993. He received the B.S. degree in electrical engineering from Chungbuk National University, Cheongju, South Korea, in 2016, and the M.S. degree in electrical engineering from the Pohang University of Science and Technology (POSTECH), Pohang, South Korea, in 2018, where he is currently pursuing the Ph.D. degree.

His current research interests include AC motor control, electric vehicle, power electronic systems, and sensorless drive.

YUNKYUNG HWANG was born in Ulsan, South Korea, in 1992. He received the B.S. degree in energy engineering from Kyungpook National University, Daegu, South Korea, in 2018, and the M.S. degree in electrical engineering from the Pohang University of Science and Technology (POSTECH), Pohang, South Korea, in 2020, where he is currently pursuing the Ph.D. degree.

His current research interests include induction motor control, electric vehicle, and power electronics.

KWANGHEE NAM (Life Member, IEEE) received the B.S. degree in chemical technology and the M.S. degree in control and instrumentation engineering from Seoul National University, Seoul, South Korea, in 1980 and 1982, respectively, and the M.S. degree in mathematics and the Ph.D. degree in electrical engineering from the University of Texas at Austin, TX, USA, in 1986. From 1998 to 2000, he was the Director of the Information Research Laboratories and the Dean of the Graduate School of Information Technology, Pohang University of Science and Technology (POSTECH), Pohang, South Korea, where he is currently a Professor with the Department of Electrical Engineering. He actively involved in developing EV motors and inverters, since 1997, and led several big EV powertrain projects sponsored by major Korean companies. His current research interests include AC motor control, power converters, and motor design. He is the author of the book *AC Motor Control and Electrical Vehicle Applications*, (CRC Press, 2010). He was a recipient of the Best Transaction Paper Award from the IEEE Industrial Electronics Society, in 2000, and the Second Best Paper Award at the 2014 IEEE Energy Conversion Congress and Exposition (ECCE). He acted as the Chair of IEEE supported international conferences, and is serving currently as the President for the Korean Institute of Power Electronics (KIPE).